The SZ effect contribution to WMAP: A Cross-Correlation between WMAP and ROSAT

J.M. Diego[1], J. Silk[1], W. Sliwa[2].

[1] *University of Oxford. Denys Wilkinson Building, 1 Keble Road, Oxford OX1 3RH, United Kingdom.*
[2] *Nicolaus Copernicus Astronomical Center, Bartycka 18, 00-716 Warsaw.*

Draft version 7 March 2003

ABSTRACT

We cross-correlate WMAP and ROSAT and look for common features in both data sets. We use the power spectrum of the product maps and the cross-power spectrum to highlight a possible correlation. The power spectrum of the product maps detects a common structure with a coherence length of $\approx 2°$ while the cross-power spectrum does not show any significant deviation from 0. We look for the origin of the correlation in the power spectrum and find that most of the correlation excess is due to just one bright source in ROSAT which correlates with a 3σ peak in WMAP. Once this source is removed the correlation disappears. From the fact that we do not observe a significant correlation between the two data sets we are able to set an upper limit on the possible models. From these models, we predict the level of contamination of the SZ effect on the power spectrum of the CMB. This contribution is found to be negligible for WMAP and is expected to be very small in experiments like ACBAR or CBI, but can be important for future high resolution experiments. We also discuss possible sources of systematic errors.

Key words: cosmological parameters, galaxies:clusters:general

1 INTRODUCTION

The recent release of the WMAP data (Bennett et al. 2003) has opened a new window for studies of large-scale structure based on the well known Sunyaev-Zel'dovich effect (SZ effect) (Sunyaev & Zel'dovich, 1972). The SZ effect shifts the spectrum of the CMB photons to higher frequencies. This shift is redshift-independent and proportional to the product of the electron column density with the *average* temperature along the line of sight. The electron temperature and optical depth to Thomson scattering are particularly high inside galaxy clusters. Thus, the SZ effect is a good tracer of clusters, even for those at high redshift. Around galaxy clusters, a diffuse, possibly filamentary, distribution of hot gas is believed to be present. These filaments have not been definitively detected due to their low contrast compared with the background (either CMB or X-ray backgrounds). The same electrons which cause the SZ effect will also emit X-rays by bremsstrahlung emission. Therefore, one expects the SZ effect and the X-ray emission of galaxy clusters and filaments to be spatially correlated. Since the X-ray background and the CMB are not correlated (except at very large scales where there could be a correlation due to the integrated Sachs-Wolfe effect (Boughn et al. 1998), the cross-correlation of an X-ray map with the CMB should enhance the signal of

clusters and filaments with respect to the background. This fact motivates the present study.

We will be interested in studying the cross-correlation $SZ \otimes XR$ (where $\otimes$ stands for cross-correlation). We need to define a *statistical object* to quantify this correlation. We will use the power spectrum of the $SZ \otimes XR$ map as such an object. We will also use the so-called cross-power spectrum (cross-correlation of the Fourier modes). The advantages/disadvantages of using the power spectrum of the product and the cross-power spectrum will be highlighted in section 3.

There are several advantages to using the power spectrum and cross-power spectrum over other statistical objects. First, they contain useful information at different scales. For instance the 0 mode accounts for the correlation coefficient of the two maps. Higher modes will contain information about the fluctuations at smaller scales. The modelling of the power spectrum is also easier and it can easily account for the uncertainties in the assumptions made in the model, as we will see below. The power spectrum will also tell us something about the contribution of clusters and filaments to the CMB power spectrum. Previous papers have claimed an excess in the CMB power spectrum (Pearson et al. 2002; Bond et al. 2002). It is not yet clear whether this

excess could be caused by the SZ effect signal or just be inadequately subtracted residuals (compact sources or residual noise). An independent estimation of the SZ effect power spectrum would help to clarify this point.

The reader is encouraged to refer to the recent literature for a more detailed description of the modelling of the power spectrum. In particular he/she may find interesting the general discussion given in Cooray & Sheth (2002), a SZ-oriented discussion in Komatsu & Seljak (2002) and Zhang & Wu (2003), or an X-ray oriented vision in Diego et al. (2003). For the WMAP results, the reader should refer to Bennett et al. (2003) and for ROSAT data he/she can find all the relevant information in Snowden et al. (1997). There are also several interesting discussions of cross-correlations between CMB and X-ray data sets (Kneissl et al. 1997, Boughn et al 1998), and the expected cross-correlation between WMAP and SDSS (Peiris & Spergel 2000).

In this work the Hubble constant is set equal to 100 h km s^{-1} Mpc, with h generally taken to be 0.7.

2 WMAP VS ROSAT: CMB VS X-RAYS

Before starting any description of the model, it is useful to give a brief description of the two data sets which are going to be used here (the reader should consult the original papers for a more detailed description). WMAP data consists of 5 all-sky maps at five different frequencies (23 Ghz $< \nu <$ 94 Ghz). At low frequencies, these maps show strong galactic emission (synchrotron and free-free). The highest frequency maps (41-94 Ghz) are the cleanest in terms of galactic contaminants and will be the most interesting for our purpose. The WMAP data is presented in a special format which conserves the size of the pixels and their shape (within small deviations) over the sky. This pixelisation (HEALPIX*) is very appropriate for power spectrum computation. Within this pixelisation, the data is presented with a pixel size of $\approx$ 6.9 arcmin (Nside=512 in HEALPIX). This pixel size oversamples the beam and also is smaller than the pixel size of ROSAT. We will repixelise the maps to the next level (Nside=256, pixel $\approx$ 13.75 arcmin). This minimum scale (13.75 arcmin) will define a maximum multipole ($l = 767$) beyond which the data does not contain additional information. The units of the WMAP data are temperature fluctuations with respect to the background (ΔT).

We will focus on one basic linear combination of the WMAP data, the differenced $Q - W$ bands of the $1°$ smoothed version of the original data. This differencing completely removes the main contaminant in this work, the CMB leaving a residual dominated by galactic and extragalactic foregrounds as well as filtered instrumental noise.

On the other hand, the ROSAT All-Sky Survey data (RASS, see Snowden et al. 1997) is presented in a set of bands ($\approx 0.1 - 2$ keV). Low energy bands are highly contaminated by local emission (local bubble and Milky Way galaxy) while high energy bands show an important contribution from extragalactic AGN's. The optimal band for our purposes will be the band R6 ($\approx$ 0.9-1.3 keV). This band is the best in

---

* available at http://www.eso.org/science/healpix.

---

terms of instrumental response, background contamination and cluster vs AGN emission. The pixel size is 12 arcmin and the units are cts/s/arcmin^2. The ROSAT maps have been *cleaned* from the most prominent point sources (AGN's above 0.02 cts/s in the R5+R6 band). However, we should note that for the above threshold (0.02 cts/s), the survey source catalogue was complete over 90 % but still smaller than 100% so there may be some point sources present in the maps of the diffuse X-ray background. We will come to this point later.

Due to the different pixel size, we have repixelised the ROSAT R6 band using HEALPIX and the same resolution level (Nside=256).

Although the R6 band is the *cleanest* in terms of galactic and AGN contamination, it still contains very strong emission coming from the galactic disk. In order to maximise the extragalactic signal, we restrict our analysis to regions outside the galactic plane. In particular, we will consider only a *clean* portion of the sky above $b = 40°$ and $70° < \ell < 250°$ which will also exclude the contribution from the north-galactic spur. This *optimal* area of the sky covers $\approx 9\%$ of the sky.

As mentioned in the introduction, a CMB map will contain distortions due to the SZ effect and an X-ray map will show some structure due to the same hot and dense plasma. However, there are many differences between the two emission sources which should be well understood before modelling the power spectrum of the cross-correlation. The distortions in the CMB map are proportional to the integral of the electron density times its temperature along the line of sight. When we take the integrated signal across the area of the plasma cloud, we find that (assuming $T = const$),

$$S_{SZ} = S_o \frac{TM}{D_a(z)^2} \qquad (1)$$

That is, the total emission depends only on the total pressure of the plasma cloud, but not on its geometry. The constant F_o includes all the proportionality constants (baryon fraction, frequency dependence and units, $\Delta T/T$ or mJy). On the contrary, the X-ray emission by the same plasma is proportional to an integral involving the square of the electron density times the square-root of its temperature. If we now calculate the total emission from the cloud of plasma we find the surprising result that the total emission depends very much on the geometry of the cloud. This comes from the fact that the bremsstrahlung X-ray emission involves two particles and therefore the denser parts of the cloud will have a much larger emission rate than the less dense parts. Meanwhile, the SZ effect can be very well modelled if we only know the amount of gas and its temperature, whereas the X-ray emission involves one more unknown degree of freedom, the density profile of the electron cloud which is poorly known. Actual observations of the X-ray emission in galaxy clusters find that the observed total emission cannot be simply reconciled with the predictions from analytical models. We need to include additional phenomena in the models (pre-heating, cooling flows, clumpiness) to explain this discrepancy. This suggests that pure modelling of the X-ray emission can produce predictions which are far away from the observations. In this paper, we will try to overcome this problem by modelling the X-ray emission using phe-

nomenological forms which match the observations. Thus, we will model the total X-ray emission as;

$$S_{XR} = \frac{Lx}{4\pi D_l(z)^2} = \frac{L_o T^\alpha (1+z)^\psi}{4\pi D_l(z)^2} \qquad (2)$$

where Lx is the X-ray luminosity and the parameters L_o, α and ψ will be chosen to match the observed $L_x - T$ relation. In modelling the temperature in both equations (1 and 2) we will use the relation,

$$T = T_o M^\beta (1+z)^\phi \qquad (3)$$

The specific values of T_o, β and ϕ will be discussed later. The X-ray flux must be converted into the flux units of the R6 band. We do this following Diego et al. (2003).

3 POWER SPECTRUM OF THE PRODUCT AND CROSS-POWER SPECTRUM

The previous discussion relates the mm and the X-ray emission from the same plasma. However, our two data sets will include other components which could (and eventually will) show a spatial correlation between the two maps. A good way to highlight this correlation is by using the power spectrum of the product map and compare it with the power spectrum of the product of two statistically similar maps with no spatial correlation between them. This can be done by just rotating one of the maps (so the spatial correlation disappears). This approach is different to the standard one where one looks for correlations in the Fourier modes (cross-power spectrum). This second approach renders good results when the signal responsible for the correlation is extended. When one looks for correlations due to compact signals, the former approach renders better results. The reason is that a cross-correlation of the Fourier modes is equivalent to a convolution of the two maps. In this convolution, the spatial information of the compact sources is partially lost since it is *diluted* over the Fourier plane. In the absence of noise, both approaches should give the same results. However, when the noise is present, the correlation between the Fourier modes is only evident at large scales since at small scales, their correlation produces a signal which is much weaker than the oscillations (around 0) of the non-correlated noise. On the contrary, by multiplying the two maps in real space we make full use of the spatial correlation between the sources before going to the Fourier space. We have tested the performance of the power spectrum of the product against the cross-power spectrum of the Fourier modes with simulations which try to reproduce the characteristics of our data sets. Our results confirm that the power spectrum of the product maps is more sensitive than the standard cross-power spectrum. However, the power spectrum of the product has one drawback. It is very sensitive to *single* fluctuations in both maps. If we have a 5σ fluctuation in each map, then after multiplying the final fluctuation will much larger and may dominate the power spectrum. On the contrary, the cross-power spectrum is much more *stable*. In this work we will look at both quantities.

Before modelling the power spectrum of the product maps and their cross-power spectrum, it is interesting to discuss what else we expect to contribute. We can split our data

in two components, signal and residual. The signal in our case will be the emission (mm or X-ray) of galaxy clusters and filaments. The residual will include all the rest. That is, the CMB, all the foregrounds, unresolved radio sources and the instrumental noise for the case of the WMAP data and non-removed AGN's (see above), galactic emission, residuals left after corrections for solar flares, and/or cosmic rays plus a small contribution coming from intrinsic instrumental read-out noise in the ROSAT case.

When we cross-correlate the WMAP and ROSAT maps, there will be a contribution to the power spectrum coming from these residuals. Even if the WMAP and ROSAT residuals are not correlated, the power spectrum of the product map will show *features* which are common to some (or both) of the residuals. On the other hand, if the maps are not correlated, the cross-power spectrum will oscillate around 0 (with mean value ≈ 0). The easiest way of thinking of this is by imagining what should we expect in a simple toy model. Let us take for instance two maps A, and B which are not correlated (correlation coefficient $= 0$). Model A will be an all-sky map containing a dipole (just the dipole) and model B an all-sky map containing pure white Gaussian noise. If we cross-correlate the maps, we will find that the cross correlation coefficient (the monopole) is 0 as expected but the product map will show a strong dipole which will show up in the power spectrum of the product maps. On the other hand, the cross-power spectrum will oscillate around 0 showing that the maps are non-correlated.

3.1 Power spectrum of the product maps

When we multiply WMAP with ROSAT the total power spectrum will be the sum of two power spectra:

$$C_l^\otimes = C_{l,\xi}^\otimes + C_{l,c}^\otimes \qquad (4)$$

where $C_l^\otimes$ is the power spectrum of the product maps, $C_{l,\xi}^\otimes$ the power spectrum of the product of the residuals and $C_{l,c}^\otimes$ the power spectrum due to the cluster (and filament) correlations between the mm and X-ray band. The previous equation follows from the assumption that the cluster and filament signal is not correlated with the residual (all the signal which is not due to clusters). This discussion can be illustrated with a simple example. In figure 1 we consider a case where the CMB data contains just CMB (simulated) and the SZ effect. We cross-correlate this simulated map with the real ROSAT R6 data and with a randomised version of ROSAT. The SZ effect emission was simulated based on a catalogue of more than 2700 Abell & Zwicky galaxy clusters. The masses were computed from the richness and the distances by calibrating the magnitude of the 10th brightest member with the known distances of 700 clusters. SZ effect total fluxes were computed using equation 1. The noise of ROSAT was simulated by randomising the positions of the pixels of ROSAT. This technique has the advantage that the noise map has exactly the same pdf as the original data but no real structure. From figure 1 we can see how in fact the cross-correlation of the CMB map plus SZ_{Abell} with the ROSAT has significant power at small scales. When we cross-correlate with the randomised ROSAT this power disappears (dotted line). The same thing happens when we

cross-correlate ROSAT with a 180° rotation of the Abell cat-alogue plus CMB (dashed line). It is important to note that even in the case where we cross-correlate $CMB + SZ_{Abell}$ with the *ROSAT noise*, the resulting map still has structure at large scales.

Although not discussed in this work, the main contribution to the power spectrum of the cross-correlated map will come from nearby clusters (see Diego et al. 2003).

For modelling the term $C_{l,c}^{\otimes}$, we only need to know some-thing about the cluster distribution and their signal in each band. Basically, this term will be the contribution of two terms,

$$C_{l,c}^{\otimes} = C_{l,c}^{\otimes}(2h) + C_{l,c}^{\otimes}(1h) \quad (5)$$

The first term accounts for the two-halo contribution and it includes the contributions to the power spectrum due to the cluster-cluster spatial correlation. This term will be signifi-cant only at very large scales. However, as we will see later, the power spectrum at large scales will be dominated by the power spectrum of the cross-correlated residuals, $C_{l,\xi}^{\otimes}$. Also, the large scales will be affected by the window function of our optimal area (Sliwa et al. 2001). Therefore, the large scales ($\theta > 20°$ or $\ell < 10$)) will not be used used here. Since the modelling of the two-halo component is a rather compli-cated process involving several assumptions about the bias and its evolution and that it only contributes significantly to the large scales we will not consider the two-halo contri-bution in this work. The main contribution at small scales will come from the single-halo contribution ($C_{l,c}^{\otimes}(1h)$). This is just given by,

$$C_l = \int dz \frac{dV(z)}{dz} \int dM \frac{dN(M,z)}{dM} p_l(M,z) \quad (6)$$

where $dV(z)/dz$ is the volume element, $dN(M,z)/dM$ is the cluster mass function and $p_l(M,z)$ is the power spectrum (multipole decomposition) of the $SZ \otimes XR$ cross-correlated 2D profile of a cluster with mass M at redshift z. In this work we will assume the Press-Schechter description for the mass function (Press & Schechter 1974) although other ap-proaches could be easily incorporated into the previous for-mula.

The term $p_l(M,z)$ can be modelled as

$$p_l(M,z) = p_o(M,z) * f(l,M,z) \quad (7)$$

where p_o is just the total signal of the $SZ \otimes XR$ cross-correlated 2D profile and $f(l,M,z)$ contains the multipole dependence which depends only on the geometry of the 2D profile. This term can be fitted numerically by the following expression,

$$f(l,M,z) = \frac{1}{2}\left(\exp(-\Sigma_{l,R_c}) + \exp(-\sqrt{\Sigma_{l,R_c}})\right) \quad (8)$$

with,

$$\Sigma_{l,R_c} = l^2 R_c^{2/(0.97+0.68e-4/R_c)} \quad (9)$$

where the core radius, R_c, is given in rads The specific shape of $f(l,M,z)$ will depend only on the geometry of the cluster. Equations (8) and (9) are valid for a β-model with $\beta = 2/3$ truncated at the virial radius. The effects of the profile will be discussed later. The central density is irrelevant for us since we normalise the total signal using equations 1 and 2.
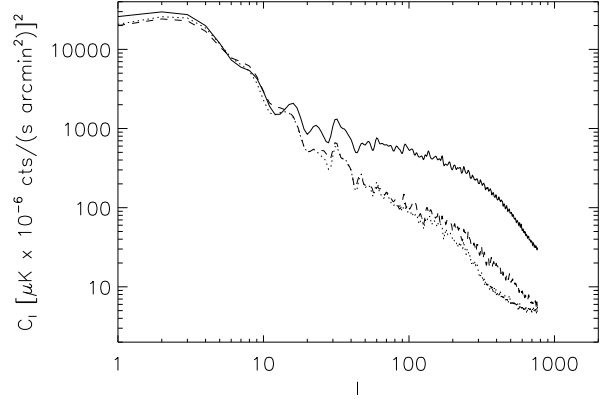

Figure 1. The thin solid line is the power spectrum of a cross correlated CMB simulation plus a SZ effect simulation (based on a catalogue of Abell clusters) with the ROSAT R6 band data. In the dashed line we rotate the simulated SZ effect 180 deg in the direction E-W. The dotted line is the power of the cross-correlation between $CMB + SZ_{Abell}$ and a random realisation of the ROSAT data.

The only relevant parameters will be the core radius and the ratio $p = virial/core$ radius which we set to $p = 10$ and will discuss other options later.

In terms of observable quantities, p_o can be expressed as,

$$p_o(M,z) = 4\pi|Mean|^2 \quad (10)$$

where $Mean$ is the mean signal of the cluster on the sky. That is, the product of the sky-averaged mm signal times the X-ray signal.

$$S_{SZ}(\theta) = S_{SZ}\frac{A(\theta)}{Tot(A)} \quad (11)$$

$$S_{XR}(\theta) = S_{XR}\frac{B(\theta)}{Tot(B)} \quad (12)$$

whre the terms S_{SZ} and S_{SZ} are given by equations 1 and 2 respectively. The factors $A(\theta)/Tot(A)$ and $B(\theta)/Tot(B)$ account for the profile dependence of the signal. It is impor-tant to include them because, as compared with the power spectrum in the X-rays or the SZ effect (see Diego et al. 2003), $Mean$ will depend on the assumed profile. From the two previous equations, it is easy to show that,

$$Mean = \frac{S_{SZ}S_{XR}}{4\pi}\frac{Tot(AB)}{Tot(A)Tot(B)} \quad (13)$$

where $Tot(AB)$ is the integrated 2D profile of the cross-correlated $SZ \otimes XR$ image while $Tot(A)$ and $Tot(B)$ are the integrated profiles of the SZ effect and X-ray 2D pro-files respectively. Then, the only additional information we need to compute the cluster $SZ \otimes XR$ power spectrum is to define the scaling relations (equations 1 and 2) and give an expression for the core radius as a function of mass and redshift. For the scaling relations, we will use the best fit-ting model found in Diego et al. (2001). The advantage of using this model is that the combinations of parameters of this model produce a good fit to several cluster data sets (mass function, temperature function, X-ray luminosity and flux functions). Later we will discuss other alternatives. For

Table 1. Reference model. All numbers are dimensionless except L_o which is given in units of $10^{42}h^{-2}erg/s$, T_o which is in keV and r_o in $h^{-1}Mpc$. ϕ and ψ have been fixed to 1 since we are not sensitive to them. This model is in perfect agreement with several cluster data sets (Diego et al. 2001, Diego et al. 2003)

Ω_m	σ_8	Γ	L_o	α	T_o	β	r_o	p
0.3	0.8	0.2	1.12	3.2	9.48	0.75	0.13	10

the core radius, we will assume that this is given by the expression;

$$R_c = \frac{R_v}{p} = r_o M_{15}^{1/3}(1+z)^{-1}h^{-1}Mpc \qquad (14)$$

We will assume that the core radius is a constant fraction of the virial radius. We will take this fraction (concentration parameter) as $p = 10$ ($R_v = pR_c$). We summarise our *reference* model in table 1. We will use this model just for illustration purposes.

Once we have defined our model, we can compute the power spectrum (equation 6).

3.2 Cross-power spectrum

The $SZ \otimes XR$ cross-power spectrum of ($C_\ell(X)$) is defined as;

$$C_\ell(X) =< a_{\ell m}^{SZ} a_{\ell m}^{XR^*} > \qquad (15)$$

where $a_{\ell m}^{SZ}$ are the coefficients of the spherical harmonics decomposition of the SZ effect map and $a_{\ell m}^{XR^*}$ are the complex conjugate of the coefficients of the cluster XR map. The modelling of the cross-power spectrum is difficult since it involves the direct modelling of the $a_{\ell m}$ instead of their dispersion, C_ℓ, however, under certain special conditions this complicated modelling can be simplified enormously.

If we impose that the cluster XR map is proportional to the SZ effect map, then their corresponding $a_{\ell m}$'s will obey the same proportionality and the problem of modelling the cross-power spectrum can be solved easily. We have to point out that the above situation does not occur in reality but we will show how the previous assumption is a good approach. If we look at equations 1 and 2 we realize that in the particular case where we take $T \propto M^{0.54}$ (Nevalainen et al. 2000) and $L_x \propto T^{2.85}$ (e.g Markevitch 1998, Arnaud & Evrard 1999), then, at low redshift the total SZ effect signal is proportional to the cluster X-Ray flux. When we calculate the flux in the R6 band and transform flux to cts/s (see Diego et al. 2003) we introduce an extra dependence on the cluster temperature which breaks the proportionality. However, this extra dependence with T is weak for clusters above ≈ 3 keV and could be easily compensated with a slightly different exponent in the $L_x - T$ relation. Also, there is a different dependency with redshift in the SZ signal and X-ray flux, but at small redshift ($z < 0.1$, $D_a(z) \approx D_l(z)$) the redshift does not play a significant role. Also in Diego et al. (2003), the authors shown that the X-ray cluster power spectrum is dominated by the low redshift population and the intermediate mass clusters ($T \in [3, 10]$ keV). under these circumstances, we can make use of the above *cosmological coincidence* ($a_{\ell m}(XR) \propto$
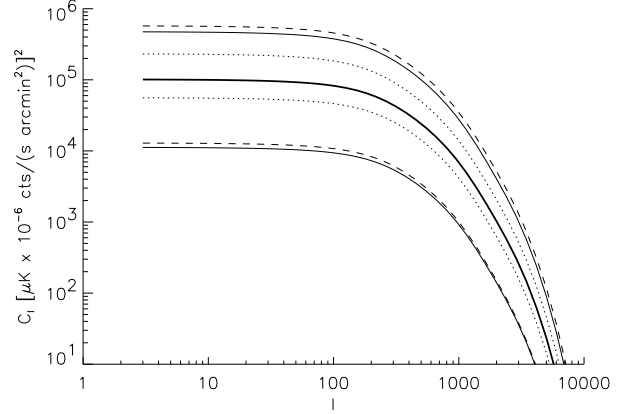

Figure 2. Dependence of the power spectrum with the cosmological parameters. The thick solid line is the reference model of table 1. Dashed line shows the change in power when we change σ_8 0.1 units with respect to the reference model ($\sigma_8 = 0.7$ bottom, $\sigma_8 = 0.9$ top). Thin solid lines show the change when we vary Ω_m 0.1 units ($\Omega_m = 0.2$ bottom and $\Omega_m = 0.4$ top). Dotted lines show the effect of changing Γ in 0.05 units, ($\Gamma = 0.15$ top and $\Gamma = 0.25$ bottom).

$a_{\ell m}(SZ)$ when $T \propto M^{0.54}$ and $L_x \propto T^{2.85}$) and we can easily model the cross-power spectrum.

$$C_\ell(X) =< a_{\ell m}^{SZ} a_{\ell m}^{XR^*} >= KC_\ell^{SZ} = \sqrt{C_\ell^{XR} C_\ell^{SZ}} \qquad (16)$$

where K is the proportionality constant, $a_{\ell m}^{XR} = Ka_{\ell m}^{SZ}$ and we have used the fact that $C_\ell^{XR} = K^2 C_\ell^{SZ}$. The properties of the cross-power spectrum are then a combination of the properties of the individual spectra of the SZ effect and the X-ray. These properties have been discussed in the literature and we will not repeat them again (Komatsu & Seljak 200, Zhang & Wu 2003, Diego et al. 2003). However, we will explore the properties of the power spectrum of the product maps in more detail in the next section.

4 THE POWER SPECTRUM OF CMB⊗X-RAY AS A PROBE

From the discussion in the previous sections, we have seen that we could expect a cluster signal in the the power spectrum of $WMAP \otimes ROSAT$. This signal can be used to constrain the cosmological model and/or the cluster physics ($T - M$, $L_x - T$ relations, and cluster geometry). Using equation 6, we can predict the power spectrum of clusters for a wide variety of cosmological models and different assumptions about the physics of the plasma. In figure 2 we show some examples of the dependence of the cluster power spectrum with the cosmological parameters. The dependence with the cluster physics is shown in figure 3. The power spectrum shows an important dependence with σ_8 and Ω_m and a weaker dependence with the shape parameter Γ. This plot illustrates the enormous possibilities of the power spectrum as an independent cosmological discriminator. The drawback is that the power is also very sensitive to the physics of the plasma (figure 3) so one must be very careful with the selection of the scaling relations and the density
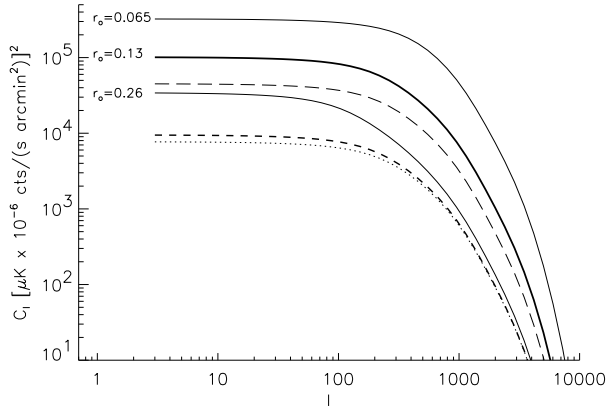
Figure 3. Dependence of the power spectrum with the cluster physics. The thick solid line is again the reference model. The two thin solid lines show the change when we take $p = 20$ ($r_o = 0.065$) and $p = 5$ ($r_o = 0.26$)). If we change from $\alpha = 3.2$ to $\alpha = 2.7$, the power spectrum changes from the solid line to the dotted line. If we change $\beta = 0.75$ to $\beta = 0.56$, the power spectrum decreases only 20% (not represented). Changing L_o to $0.7L_o$ moves the solid line to the thin long-dashed line. Finally, varying T_o to $0.7T_o$ changes the solid curve to the thick sort-dashed curve.

profile in order to not introduce a bias in the resulting cosmological parameters. However, we can turn this apparent problem into a productive way of studying the intra-cluster physics. If the cosmological model is known with some accuracy, then one can use the power spectrum as a way to constrain for instance the extension of the plasma cloud. From figure 3, it is interesting to see how when the concentration parameter changes from 5 to 20, the power increases a factor 50 (at $\ell \approx 500$). This is a unique dependence which cannot be observed when one looks at the power spectrum of clusters in the mm or X-ray band (Komatsu & Seljak 2002, Diego et al. 2003). Only when we cross correlate these bands, we can make evident the dependence of the normalisation of the power on the geometry of the cluster (see equation 13). Also interesting is to see the dependence of the power with the scaling relations. In figure 3 we only illustrate the dependence with the scaling exponents α and with the normalisation constants L_o and T_o. The dependence with ψ and ϕ will be weak since the power is dominated by low redshift clusters.

It is possible to trace back the dependence of the power spectrum on the scaling relations by just looking at equations 13, 1 and 2. In the case of L_o the dependence is just $C_l \propto L_o^2$. In the case of T_o the dependence is a little more complicated since it also enters in the band correction ($B_{corr} = exp(E_{min}(1+z)/kT) - exp(E_{max}(1+z)/kT)$) for bremsstrahlung, $C_l \propto (T_o * B_{corr})^2$. The power shows a weak dependence with the β exponent. A smaller exponent β will increase the temperature of the temperature of clusters with masses below $M_{15} = 10^{15}h^{-1}M_\odot$ and will decrease the temperature of clusters above that mass. The total luminosity of the clusters with $M > M_{15}$ will also increase as T^α. However, this increase is compensated by the smaller X-ray band-correction which peaks at $T \approx 1keV$ and decreases for larger temperatures. The strong dependence of the power

with α is easier to follow since in this case the temperature does not change (and neither does the band-correction). In this case, a smaller α will produce a smaller X-ray luminosity (Lx) and consequently a smaller power ($C_l \propto L_x^2$).

5   THE WMAP⊗ROSAT POWER SPECTRUM AND CROSS-POWER SPECTRUM

In order to maximise the signal-to-noise ratio, we have created a new template of WMAP based on a linear combination of some of its bands. Since the CMB is frequency-independent, two maps at two different frequencies which have been filtered with the same beam will contain exactly the same amount of CMB per pixel. In our case, the CMB is going to be the mayor contaminant so we should try to remove it. This can be done easily if we just subtract one band from the other. In our case we will subtract the W band from the Q band map (both of them smoothed with $1°$). By doing this we will maximise, the SNR of the SZ effect with respect to the noisy background. The resulting map will have a linear combination of the filtered noise of the two bands, plus foregrounds plus the SZ effect. The last one will have a signal proportional to the Compton parameter times a factor, $Correction(Q - W)$, equal to,

$$Correction(Q - W) = \frac{\int_Q f(\nu)d\nu}{\Delta\nu_Q} - \frac{\int_W f(\nu)d\nu}{\Delta\nu_W} \qquad (17)$$

where the integrals are over the corresponding bandwidths ($\Delta\nu$) and $f(\nu)$ is the well knwon frequency dependence of the SZ effect. On the other hand, since the maps have been smoothed, when we cross-correlate the (Q-W) band map with ROSAT, we have to keep in mind that, after smoothing, the 2D profile of the clusters in the CMB map will have a 2D profile different from the 2D β-model. We will also include this fact in our calculations. Finally, as we pointed out before, we will consider only a *clean* portion of the sky ($b > 40°$ $70° < \ell < 250°$) to minimise the correlations introduced by the galaxy.

The power spectrum of (Q-W) $WMAP \otimes ROSAT$ is shown in figure 4. The main conclusion from this plot is that there is an excess in power with respect to the background level at scales smaller than 2 degrees ($\ell \approx 100$). The background level can be determined by rotating one of the maps. The structure due to the correlation between the maps will disappear beyond the coherence length. From figure 4, it is clear that this coherence length must be around 2 degrees (or smaller) since at larger angular separations the power reaches the background level (bottom dotted lines). When the rotation is smaller than 0.2 degrees, we are rotating over an angle which is smaller than the pixel size (13.74 arcmin). In this case the power spectrum is the same as in the case with 0 rotation. A coherence length of 2 degrees would be in agreement with the measured cross-correlation between the angular position of Abell clusters and the intensity of the X-ray background (Soltan et al. 1996). which extends up to several degrees.

In the same plot, we also show the case when we cross-correlate WMAP with a random realisation of ROSAT
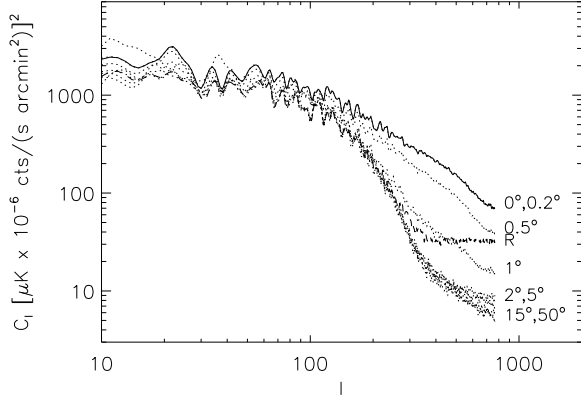
Figure 4. power spectrum of $WMAP \otimes ROSAT$ (solid line). The dotted lines are the power spectra when we rotate WMAP between $0.2°$ and $50°$. The dashed line (labelled R in the plot) is the power of WMAP cross-correlated with a random realisation of ROSAT.

(dashed line). In this case, the power spectrum has less power than the $WMAP \otimes ROSAT$ power but it has more power than the background level (bottom dotted curves). This is easy to understand since the random ROSAT realisation does not contain any structure at all (flat power spectrum) while the real ROSAT data does have that structure (which suppresses power at small scales compared with the random map).

However, as we said earlier, the drawback of the power spectrum is that it is very sensitive to single large fluctuations in the data. Unfortunately, we have one of these fluctuations. Although apparently clean of bright point sources, the map of the diffuse X-ray background has a very large fluctuation in our area of the sky which was not subtracted from the original maps. This source (MRK 0421) is a very powerful X-ray source (≈ 26 cts/s in ROSAT broadband). This blazar is also known as a strong radio source (≈ 1 Jy at 1.4 Ghz). However, it is not one of the ≈ 200 sources in the WMAP point source catalogue. In the (Q-W) map, it appears as a $> 3\sigma$ peak at the position of the blazar. When multiplied with the ROSAT map, the blazar produces a very large fluctuation which dominates the power spectrum. If we rotate one of the maps, the fluctuation weakens and the excess in power disappears. When we remove the blazar from the diffuse X-ray maps, we do not observe any significant excess in power relative to the background (rotations). In figure 5 we show the result once we remove the blazar. We have also removed 12 more pixels in ROSAT which are associated to very bright sources (one non-removed X-ray star (RBS 0768) and the Leo cluster, Abell 1367).

When we look at the cross-power spectrum, we do not observe any significant signal. This is not surprising since, the cross-power spectrum is more stable than the power spectrum of the product maps but is also less sensitive to correlations at small scales. Furthermore, the range of ℓ's at which is more sensitive (low ℓ's) is affected by the window of our selected area of the sky. We show the cross-power spectrum in figure 6. The power spectrum shows strong fluctuations around 0. We have rebinned the cross-power spectrum
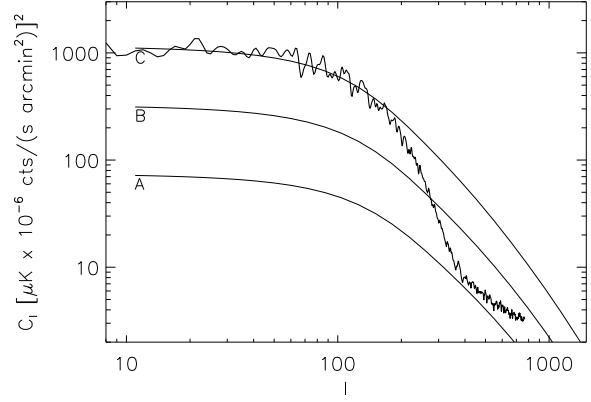

Figure 5. Power spectrum of (Q-W) band after removing the 16 brightest pixels in ROSAT. The excess in power disappears (power spectrum similar to the background case). The thin solid lines are the predicted signals for the models in table 2.

Table 2. These three models are compared wit the observed power spectrum in band (Q-W) (thick line) in figure 5.

Model	Ω_m	σ_8	L_o	α	T_o	β	r_o	p
A	0.3	0.8	1.5	2.85	8.0	0.54	0.15	10
B	0.3	0.9	1.5	2.85	8.0	0.54	0.15	10
C	0.3	1.0	1.5	2.85	8.0	0.54	0.15	10

in bins of $\Delta\ell = 20$ in order to get a *smooth* version but still is difficult to see any significant deviation from 0.

Although we do not detect any signal neither with the power spectrum of the product maps nor the cross-power spectrum, we can still use this fact to set some constraints on the model. In figures 5 and 7 we compare the measured power and cross-power with three different models where we
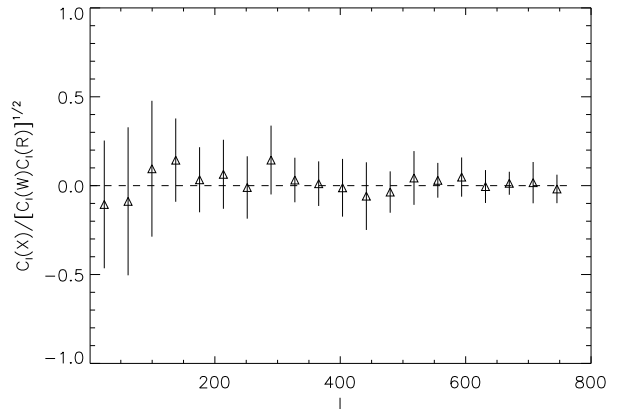

Figure 6. Binned ($\Delta\ell = 20$) cross-power spectrum of WMAP(Q-W) times ROSAT(R6). The cross-power spectrum has been divided by the factor $\sqrt{C_\ell(WMAP)C_\ell(ROSAT)}$ to make the fluctuations at large ℓ more evident.
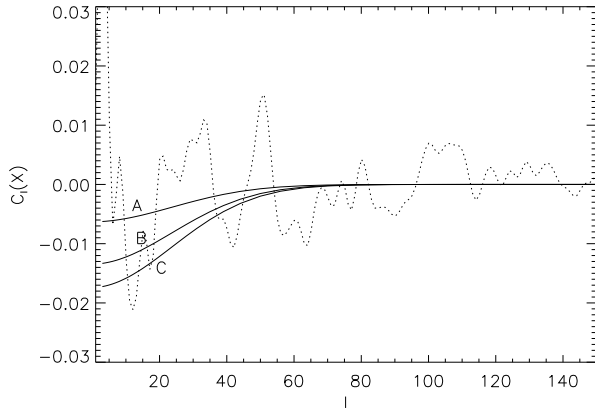
Figure 7. Cross-power spectrum (dotted line) compared with the three models in table 2.

change the parameter σ_8 (the models are listed in table 2). This simple comparison tell us that the only way to accommodate models with high σ_8 is by reducing the luminosity of the clusters, and/or their temperature and/or increasing their sizes (decreases the power at small scales). They could also be accommodated if the SZ effect is significantly contaminated by point sources so the net distortion in the CMB is smaller than if the cluster signal is just pure SZ effect.

6   CONCLUSIONS

Using the power spectrum of the product maps, we have detected a common structure to the WMAP and ROSAT data. However, the correlation disappears when we remove the blazar MRK 0421 from the ROSAT data. We obtain the same negative result (no significant correlation) using the cross-power spectrum. However, this fact can be used to set limits on the model. This limits should be robust unless the SZ effect is significantly contaminated by point source emission (which compensates the negative SZ effect distortion) in which case the absence of any correlation could be explained by this fact.

We model the power spectrum of the product map and the cross-power spectrum with an intuitive model based on empirical observations (cluster scaling relations) rather than pure modelling of the electron density. Our predictions are then relatively robust. We have shown how the cluster power spectrum of CMB⊗X-ray experiments can be a powerful technique in future cosmological studies but can also be useful for studying the physics of the intra-cluster plasma.

We found that different assumptions about the model lead to different fits to the data. In particular, high values of σ_8 seem to be difficult to reconcile with the absence of significant correlation.

This absence of significant correlation can also be used to rule out the possibility that the excess in ACBAR and CBI is due to SZ effect. We illustrate this point in figure 8 where we compare the power spectrum of the SZ effect for the models in table 2 with the recent estimate of the CMB power spectrum by WMAP (solid line) and with estimates from ACBAR (Kuo et al. 2003) and CBI (Pearson et al. 2002).
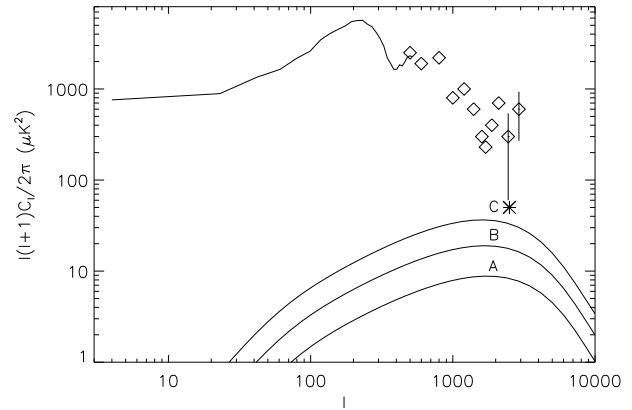

Figure 8. Current estimates of the CMB power spectrum compared with predicted SZ effect power spectrum (R-J) for the models in table 2. The top solid line is a rebinning (10 bins) of the original WMAP CMB power spectrum. The symbols are current estimates by CBI and ACBAR (error bars have been omitted except in the last two points). The last three symbols at $\ell \approx 3000$ are the estimated power spectrum at high ℓ by CBI (top), ACBAR (middle) and the expected CMB power spectrum for a standard model (bottom star). Solid lines represent the models in table 2.

From this plot we can conclude that the fact that we do not observe a correlation between WMAP and ROSAT implies that the SZ effect power spectrum should not contribute significantly to any of these experiments.

7   ACKNOWLEDGEMENTS

REFERENCES

Arnaud M., & Evrard A.E. 1999, MNRAS, 305, 631.
Bennet et al. (more than 8 authors). 2003, submitted, astro-ph/0302207
Bond J.R., et al. (more than 8 authors). 2002, ApJ submitted. astro-ph/0205386.
Boughn S. P., Crittenden R. G., Turok N., 1998, New Astronomy, vol. 3, no. 5, p. 275.
Cooray A., Sheth R., 2002,Physics Reports, Vol 372, Issue 1, 1.
Diego J.M., Martínez-González E., Sanz J.L., Cayón L., Silk J. 2001, MNRAS, 325, 1533.
Diego J.M., W. Sliwa, J. Silk, X. Barcons, W. Voges. 2003, MNRAS submitted. astro-ph/0302067.

Górsky K.M., Hivon E, Wandelt B.D., 1999, in Proceedings of the MPA/ESO Cosmology Conference "Evolution of Large-Scale Structure", eds. A.J. Banday, R.S. Sheth and L. Da Costa, PrintPartners Ipskamp, NL, pp. 37-42. (astro-ph/9812350).

Kneissl R., Egger R., Hasinger G., Soltan A.M., Trümper J., 1997, A&A, 320, 685.

Komatsu E., & Seljak U., T., 2002, MNRAS, 336, 1256.

Kuo et al. (more than 8 authors). 2003, ApJ submitted. astro-ph/0212289.

Markevitch M., 1998, ApJ, 504, 27.

Nevalainen J., Markevitch M., Forman W., 2000, ApJ, 532, 694.

Pearson et al. (more than 8 authors). 2002, ApJ submitted. astro-ph/0205384.

Peiris H.V., Spergel D.N., 2000, ApJ 540, 605.

Press W.H., Schechter P., 1974, ApJ, 187, 425.

Sliwa W., Soltan A.M., Freyberg M.J., 2001, A&A, 380, 397.

Snowden S.L., Egger R., Freyberg M.J., McCammon D., Plucinsky P.P., Sanders W.T., Schmitt,J. H.M.M., Truemper J., Voges W. 1997, ApJ, 485, 125.

Soltan A.M., Hasinger G., Egger R., Snowden S., Trümper J.,

Sunyaev R.A., Zel'dovich Ya, B., 1972, A&A, 20, 189.

Zhang Y-Y., Wu X-P., 2003, ApJ, 583, 529.